Research Article

Nuclear and mitochondrial genomes of the hybrid fungal plant pathogen *Verticillium longisporum* display a mosaic structure

Authors: Jasper R.L. Depotter[1,2†], Fabian van Beveren[1†], Grardy C.M. van den Berg[1], Thomas A. Wood[2‡], Bart P.H.J. Thomma[1*‡], Michael F. Seidl[1*‡]

[1]Laboratory of Phytopathology, Wageningen University, Droevendaalsesteeg 1, 6708 PB Wageningen, The Netherlands

[2]Department of Crops and Agronomy, National Institute of Agricultural Botany, Huntingdon Road, CB3 0LE Cambridge, United Kingdom

† These authors contributed equally to this work

‡ These authors contributed equally to this work

*For correspondence:

Bart P.H.J. Thomma, Laboratory of Phytopathology, Wageningen University, Droevendaalsesteeg 1, 6708 PB Wageningen, The Netherlands. Tel. 0031-317-484536, e-mail: bart.thomma@wur.nl

Michael F. Seidl, Laboratory of Phytopathology, Wageningen University, Droevendaalsesteeg 1, 6708 PB Wageningen, The Netherlands. Tel. 0031-317-484536, e-mail: michael.seidl@wur.nl

ABSTRACT

Allopolyploidization, genome duplication through interspecific hybridization, is an important evolutionary mechanism that can enable organisms to adapt to environmental changes or stresses. This increased adaptive potential of allopolyploids can be particularly relevant for plant pathogens in their quest for host immune response evasion. Allodiploidization likely caused the shift in host range of the fungal pathogen plant *Verticillium longisporum*, as *V. longisporum* mainly infects Brassicaceae plants in contrast to haploid *Verticillium* spp. In this study, we investigated the allodiploid genome structure of *V. longisporum* and its evolution in the hybridization aftermath. The nuclear genome of *V. longisporum* displays a mosaic structure, as numerous contigs consists of sections of both parental origins. *V. longisporum* encountered extensive genome rearrangements, whereas the contribution of gene conversion is negligible. Thus, the mosaic genome structure mainly resulted from genomic rearrangements between parental chromosome sets. Furthermore, a mosaic structure was also found in the mitochondrial genome, demonstrating its bi-parental inheritance. In conclusion, the nuclear and mitochondrial genomes of *V. longisporum* parents interacted dynamically in the hybridization aftermath. Conceivably, novel combinations of DNA sequence of different parental origin facilitated genome stability after hybridization and consecutive niche adaptation of *V. longisporum*.

Key words: whole-genome duplication, allopolyploidy, genomic rearrangement, Verticillium stem striping, Verticillium wilt, *Brassica*

INTRODUCTION

Whole-genome duplication (WGD) is an important evolutionary mechanism that facilitates environmental adaptation (Van de Peer et al. 2017; Mallet 2005). The duplication of genomic content increases genomic plasticity, leading to an augmented adaptive potential of organisms that underwent WGD. Consequently, polyploids have been associated with increased invasiveness (te Beest et al. 2012) and resistance to environmental stresses (Lohaus & Van de Peer 2016). For instance, numerous plant species that survived the Cretaceous-Palaeogene mass extinction, 66 million years ago, underwent a WGD which is thought to have contributed to their increased survival rates (Vanneste et al. 2014a; Vanneste et al. 2014b). Both genome copies involved in WGD may have the same species origin, i.e. autopolyploidization, or originate from different species as a result of interspecific hybridization, i.e. allopolyploidization. In general, allopolyploids are believed to have a higher adaptive potential than autopolyploids due to the increased genetic divergence between the chromosome sets.

The impact of allopolyploidization has mainly been investigated in plants, as approximately a tenth of all plant species consists of allopolyploids (Barker et al. 2015). In contrast, allopolyploidization in fungi is far less intensively investigated (Campbell et al. 2016). Nonetheless, allopolyploidization impacted the evolution of numerous fungal species, including the economically important baker's yeast *Saccharomyces cerevisiae* (Marcet-Houben & Gabaldón 2015). The increased adaptive potential enabled allopolyploid fungi to develop desirable traits that can be exploited in industrial bioprocessing (Peris et al. 2017). For instance, at least two recent hybridization events between *S. cerevisiae* and its close relative *Saccharomyces eubayanus* gave rise to *Saccharomyces pastorianus*, a species with high cold tolerance and good maltose/maltotriose utilization capabilities, which is exploited in

the production of lager beer that requires barley to be malted at low temperatures (Gibson & Liti 2015).

Allopolyploid genomes experience a so-called “genome shock” upon hybridization, inciting major genomic reorganizations that can manifest by genome rearrangements, extensive gene loss, transposon activation, and alterations in gene expression (Doyle et al. 2008). These early stage alterations are primordial for hybrid survival, as divergent evolution is principally associated with incompatibilities between the parental genomes (Matute et al. 2010). Allopolyploids benefit from a thorough re-organization where negative interactions between the parental genomes are purged. Frequently, heterozygosity is lost for many regions in the allopolyploid genome (Mixão & Gabaldón 2018). This can be a result of the direct loss of a duplicated gene copy through deletion or gene conversion, a process where one of the copies substitutes its homeologous counterpart (McGrath et al. 2014). Gene conversion and the homogenization of complete chromosomes played a pivotal role in the evolution of the osmotolerant yeast species *Pichia sorbitophila* (Louis et al. 2012). In total, two of its seven chromosome pairs consist of partly heterozygous, partly homozygous sections, whereas two chromosome pairs are completely homozygous. Gene conversion may eventually result in chromosomes consisting of sections of both parental origins as “mosaic genomes” (Stukenbrock et al. 2012). However, mosaic genomes can also arise through recombination between chromosomes of the different parents, such as in the hybrid yeast *Zygosaccharomyces parabailii* (Ortiz-Merino et al. 2017).

Plant pathogens are often thought to evolve while being engaged in arms races with their hosts; pathogens evolve to evade host immunity while plant hosts attempt to intercept pathogen ingress (Cook et al. 2015). Due to the increased adaptation potential, allopolyploidization has been proposed as a potent driver in pathogen evolution (Depotter et al. 2016b). Allopolyploids often have different pathogenic traits than their parental lineages,

such as higher virulence (Husson et al. 2015; Brasier & Kirk 2001) and shifted host ranges (Inderbitzin et al. 2011b; Zeise & Tiedemann 2002). Within the fungal genus *Verticillium*, allodiploidization resulted in the emergence of a novel pathogen on brassicaceous plants; *Verticillium longisporum* (Inderbitzin et al. 2011b; Depotter et al. 2017b). Similar to haploid *Verticillium* spp., *V. longisporum* is thought to have a predominant asexual reproduction as a sexual cycle has never been described and populations are not outcrossing (Depotter et al. 2017b; Short et al. 2014). *V. longisporum* is sub-divided into three lineages, each representing a separate hybridization event (Inderbitzin et al. 2011b). The economically most important lineage is A1/D1 that originates from hybridization between *Verticillium* species A1 and D1 that have hitherto not been found in their haploid states. *V. longisporum* lineage A1/D1 is the main causal agent of Verticillium stem striping on oilseed rape (Novakazi et al. 2015) and its economic importance as emerging pathogen is increasing worldwide (Depotter et al. 2017a). A recent study revealed that lineage A1/D1 can be further divided into two genetically distinct populations, which have been named 'A1/D1 West' and 'A1/D1 East' after their geographic occurrence in Europe (Depotter et al. 2017b). Nevertheless, both populations were shown to originate the same hybridization event (Depotter et al. 2017b).

V. longisporum is assumed to have largely conserved its allodiploid state as the sizes of its sub-genomes resemble those of haploid *Verticillium* spp. (Depotter et al. 2017b; Shi-Kunne et al. forthcoming; Fogelqvist et al. 2018). Nevertheless, not all genes are present in heterozygous copies, as its nuclear ribosomal internal transcribed spacer region is derived only from one of the parents (Inderbitzin et al. 2011b). Here, we investigated the evolution of the allodiploid genome of *V. longisporum* and determined to what extent heterozygosity is lost.

MATERIAL AND METHODS

Genome analysis

Genome assemblies of the two *V. longisporum* strains (VLB2 and VL20) and *V. dahliae* strain JR2 were previously published (Faino et al. 2015; Depotter et al. 2017b). Telomeric regions were determined based on the telomeric repeat pattern: TAACCC/GGGTTA (minimum three repetitions). Furthermore, additional repeats were identified and characterized using RepeatModeler (v1.0.8). De-novo-identified repeats were combined with the repeat library from RepBase (release 20170127) (Bao et al. 2015). The exact coordinates of the repeats were extracted with the software RepeatMasker (v4.0.6) (Smit et al. 2015). Genome-wide sequence identities between *Verticillium* strains were calculated with dnadiff (Kurtz et al. 2004). Homologous genes were retrieved by nucleotide BLAST (v2.2.31+). Here, only hits with a minimal coverage of 80% with each other were selected.

Gene annotation

Verticillium isolates JR2, VLB2 and VL20 were grown for 3 days in potato dextrose broth. Total RNA was extracted based on TRIzol RNA extraction (Simms et al. 1993). cDNA synthesis, library preparation (TreSep RNA-Seq short-inser library), and Illumina sequencing (single-end 50bp) was performed at the Beijing Genome Institute (BGI, Hong Kong, China). In total, ~2Gb of filtered reads were mapped on the *Verticillium* genomes using TopHat (Trapnell et al. 2009) with Bowtie2 (Langmead & Salzberg 2012). Gene annotation was performed with the BRAKER1 1.9 pipeline (Hoff et al. 2016) using GeneMark-ET (Lomsadze et al. 2014) and AUGUSTUS (Stanke et al. 2008). Predicted genes with internal stop codons were removed from the analysis.

Parental origin determination

Sub-genomes were divided based on the differences in sequence identities between species A1 and D1 with *V. dahliae*. *V. longisporum* genomes of VLB2 and VL20 were aligned to the complete genome of *V. dahliae* JR2 using NUCmer from the MUMmer package v3.23 (Kurtz et al. 2004; Faino et al. 2015). Here, only 1-to-1 alignments longer than 10kb and a minimum of 80% identity were retained. Subsequent alignments were clustered together. The average nucleotide identity was determined for every cluster and used for sub-genome segregation.

The parental origin determination based on sequence identities of the exonic regions of genes, which was performed by BLAST (v2.6.0+). Here, hits with a minimum subject and query coverage of 80% were used. Furthermore, similar to Louis et al. (2012), differences in GC-content between homolog genes present in two copies were calculated accordingly:

dGC_{gene} = 2*GCgene / (GCgene + GChomolog)

GCgene = GC% of gene

GChomolog = GC% of homolog

dGC_{gene} = GC ratio from the mean GC% value

Gene conversion and genomic rearrangements

Double copy genes were retrieved by nucleotide BLAST (v2.6.0+) and the sequence identity determined. Here, hits with a minimum subject and query coverage of 80% were used. Nucleotide BLAST (v2.6.0+) was also used to find the corresponding homologous genes in *V. longisporum* strains VLB2 and VL20, which were present in two copies in both strains.

The VLB2 genome assembly was aligned to VL20 to find breaks in synteny using NUCmer from the MUMmer package v3.23 (Kurtz et al. 2004). Subsequent alignments were clustered if they aligned to the same contig with the same orientation and order as the reference genome. In order to confirm the breaks in synteny, filtered *V. longisporum* reads of VLB2 were aligned to the *V. longisporum* VL20 genome with the Burrows-Wheeler Aligner

(BWA) and further processed with the samtools package (v1.3.1) (Li et al. 2009). Breaks in syntenic clusters were then visualized and determined using the R package Sushi (Phanstiel et al. 2014) and the Integrative Genomics Viewer (Robinson et al. 2011). The association between breaks with repeats was tested through permutation. First, the fraction of breaks flanked by repeats was determined. Here, breaks were assigned to reside in a "repeat-rich" region if a 1 kb window around the break consisted for more than 10% of repeats. Then, the *V. longisporum* VL20 genomes was divided into windows of 1 kb using BEDTools (v2.26.0) to calculate the significance of the break/repeat association (Quinlan & Hall 2010). In total, 10,000 permutations were executed with the same amount of windows to determine the random distribution of repeat-rich regions.

Phylogenetic tree construction

The phylogenetic tree of the nuclear DNA was based on the nucleotide sequences of the ascomycete set BUSCO orthologs present in clade Flavnonexudans *Verticillium* spp. (Simão et al. 2015). In total, 1,194 genes were included and concatenated for tree construction. The mitochondrial phylogenetic tree was based on the nucleotide sequence of complete or partial mitochondrial genomes. Nuclear and mitochondrial genomes of *Verticillium* spp. other than *V. longisporum* were previously sequenced and assembled (Shi-Kunne et al. forthcoming; Faino et al. 2015; Jelen et al. 2016). Whole-genome alignments for tree construction were performed by mafft (v7.271) (default settings) (Katoh & Standley 2013; Katoh et al. 2002), and subsequently the likelihood phylogenetic tree was reconstricted using RAxML with the GTRGAMMA substitution model (v8.2.0) (Stamatakis 2014). The robustness of the inferred phylogeny was assessed by 100 rapid bootstrap approximations.

188 **RESULTS**

189 ***V. longisporum* displays a mosaic genome structure**

190 The genomes of two *V. longisporum* strains were analysed to investigate the impact of
191 hybridization on the genome structure. Previously, *V. longisporum* strains VLB2 and VL20,
192 belonging to 'A1/D1 West' and 'A1/D1 East', were sequenced with the PacBio RSII platform
193 and annotated into genomes of 72.9 and 72.3 Mb in size, respectively (Depotter et al. 2017b).
194 These genome sizes exceed double the amount of the telomere-to-telomere sequenced *V.*
195 *dahliae* strains JR2 (36.2 Mb) and VdLs17 (36.0 Mb) (Faino et al. 2015). Despite the
196 previous observation that the two *V. longisporum* strains belong to distinct populations within
197 the A1/D1 lineage, the genomes show an extremely high degree of sequence identity
198 (99.91%). We used RepeatModeler (V1.0.8) in combination with RepeatMasker to
199 determined that 14.28 and 13.90% of the *V. longisporum* strain VLB2 and VL20 genomes is
200 composed of repeats, respectively (Table 1) (Smit et al. 2015). Intriguingly, this is more than
201 double the repeat content as in *V. dahliae* strain JR2, for which 6.49% of the genome was
202 annotated as repeat using the same methodology. The *V. longisporum* genomes were also
203 screened for telomere-specific repeats (TAACCC/GGGTTA) to estimate the number of
204 chromosomes. In total, 29 and 30 telomeric regions were found in the VLB2 and VL20
205 genomes, respectively, that were consistently situated at the end of contigs, suggesting that *V.*
206 *longisporum* contains at least 15 chromosomes (Table 1). Six out of 45 and four out of 44
207 contigs in strains VLB2 and VL20, respectively, were flanked on both ends by telomeric
208 repeats and therefore likely represent complete chromosomes (Table 1). For comparison, *V.*
209 *dahliae* strains contain 8 chromosomes (Faino et al. 2015).

210 In allopolyploid organisms, parental origin determination is elementary to investigate
211 genome evolution in the hybridization aftermath. As species D1 is phylogenetically closer
212 related, and consequently has a higher sequence identity, to *V. dahliae* than species A1, *V.*

longisporum genomic regions were previously provisionally assigned to either species D1 or A1 (Depotter et al. 2017b). Here, we determined the parental origin of *V. longisporum* genomic regions more precisely. The difference in phylogenetic distance of species A1 and D1 to *V. dahliae* caused that *V. longisporum* genome alignments to *V. dahliae* displayed a bimodal distribution with one peak at 93.1% and another peak at 98.4% sequence identity that represent the two parents with a dip in between at 96.0% (Figure S1). In order to separate the two sub-genomes, regions with an average sequence identity to *V. dahliae* <96% were assigned to species A1, whereas regions with an identity of ≥96% were assigned to species D1 (Figure 1). In this manner, 36.2 Mb of *V. longisporum* strain VLB2 was assigned to species A1 and 35.7 Mb to species D1. For *V. longisporum* strain VL20, 36.3 Mb was assigned to species A1 and 35.2 Mb to species D1. Only 1.0 and 0.8 Mb of strains VLB2 and VL20 could not be aligned to *V. dahliae* and thus remained unassigned, respectively.

To trace the chromosome sets of the original parents of the hybrid, the parental origin of individual contigs was determined. In total, 8 of the 10 largest contigs of *V. longisporum* strain VLB2 as well as strain VL20 consist of regions originating from both species A1 and species D1 (Figure 1). Thus, parental chromosome sets cannot be separated from one another as *V. longisporum* apparently evolved a mosaic genome structure in the hybridization aftermath.

Genomic rearrangements are responsible for the mosaic genome

Typically, a mosaic structure of a hybrid genome can originate from gene conversion or from chromosomal rearrangements between DNA strands of different parental origin (Mixão & Gabaldón 2018). To analyse the extent of gene conversion, genes were predicted for the *V. longisporum* strains VLB2 and VL20. To aid gene annotation with the BRAKER1 1.9 pipeline (Hoff et al. 2016), ~2 Gb of filtered RNA-seq reads were generated from fungal

cultures in potato dextrose broth. In total, 19,123 and 18,784 genes were predicted for *V. longisporum* strains VLB2 and VL20 respectively, which is ~90% higher than the amount of genes that were predicted for *V. dahliae* strain JR2 in this manner (9,909 genes) (Table 1). As expected, the divergence of species A1 and D1 was also reflected at the level of gene sequences based on sequence identity and GC-content (Figure 1, S1). In total, 9,531 and 9,402 genes were assigned to the species A1 sub-genome of the strains VLB2 and VL20, respectively, whereas the number of genes in the species D1 sub-genomes was 9,468 and 9,243 for these strains, respectively (Figure 2). Thus, the amount of genes is similar in the two sub-genomes for both *V. longisporum* strains. Over 80% of the *V. longisporum* genes are present in two copies whereas, similar to *V. dahliae*, almost all genes (97-98%) are present in one copy within each of the *V. longisporum* sub-genomes. Moreover, of the 7,620 genes that are present in two copies in VLB2 and VL20, only 5 genes were found to be highly identical (<1%, nucleotide sequence identity) in VLB2, whereas the corresponding gene pair in VL20 was more diverse (>1%, nucleotide sequence identity) (Figure 3). In *V. longisporum* strain VL20, no highly identical copies were found that are more divergent in VLB2. Collectively, these findings indicate that most *V. longisporum* genes have a copy of a different parental origin and that gene conversion played a minor role in during evolution of the mosaic genome.

Considering that gene conversion played a minor role during genome evolution, the mosaic genome structure of *V. longisporum* is likely to originate from rearrangements between the chromosomes of different parental origin. To identify the location of genomic rearrangements, the genome of *V. longisporum* strain VLB2 was aligned to that of strain VL20 (Figure 4). Extensive rearrangements were observed between the two *V. longisporum* strains, as 87 putative syntenic breaks were found. In order to confirm these synteny breaks, individual long-reads of VLB2 were aligned to the VL20 genome assembly to assess if breaks

were supported by read mapping (Figure S2). In total, 60 synteny breaks could be confirmed by read mapping. As genomic rearrangements are often associated with repeat-rich genome regions, the synteny break points were tested for their occurrence in repeat-rich regions. In total, 34 of the 60 (57%) confirmed synteny break points were flanked by repeats, which is significantly more than what would be expected from random sampling (mean = 18.5%, σ = 0.05%) (Figure S3). In conclusion, it appears that genomic rearrangements, rather than gene conversion, are the main driver behind the mosaic structure of the *V. longisporum* genome.

V. longisporum loses heterozygosity through deletions

In each of the *V. longisporum* isolates, 17% of the genes occur only in a single copy. Although gene conversion played a minor role in the hybridization aftermath, loss of heterozygosity may occur through gene loss or, alternatively, single-copy genes may originate from parent-specific contributions. However, as 12% of the singly copy genes in strain VLB2 are present in two copies in strain VL20, and 16% of the single copy genes in VL20 are present in two copies in VLB2, gene deletion seems to be an on-going process in *V. longisporum* evolution since both strains are derived from the same hybridization event (Depotter et al. 2017b). Thus, in the general absence of gene conversion in the *V. longisporum* genome, loss of heterozygosity is mainly caused by deletions.

Also the mitochondrial genome has a bi-parental origin

To determine how *Verticillium* species A1 and D1 relate to other species in the clade Flavnonexudans, a phylogenetic tree was constructed based on 1,194 Ascomycota Benchmarking Universal Single-Copy Orthologs (BUSCOs) that are present in all members of *Verticillium* clade Flavnonexudans (Figure 5). Species A1 diverged before the last common ancestor of *V. alfalfa*, *V. dahliae* and *V. nonalfalfae*. In contrast, species D1 only recently

288 diverged from *V. dahliae* after the last common ancestor of *V. alfalfae*, *V. dahliae* and *V.*
289 *nonalfalfae*. In addition to genomic DNA, the *V. longisporum* clade Flavnonexudans
290 phylogeny was also determined based on mitochondrial DNA (mtDNA) (Figure 5). The
291 mitochondrial genomes of the haploid clade Flavnonexudans spp. were previously sequenced
292 and found to be between 25-27 kb in size (Shi-Kunne et al. forthcoming; Jelen et al. 2016).
293 The *V. longisporum* mtDNA was assembled along with the nuclear genome of VLB2 and
294 VL20, which resulted in a mitochondrial genome of 26.1 kb. Unanticipatedly, the
295 phylogenetic position of *V. longisporum* based on mtDNA did not correspond to the
296 previously determined phylogenetic positions of either of the parents based on the nuclear
297 DNA (Figure 5), as it appeared that *V. longisporum* diverged more recently from the *V.*
298 *alfalfae*/*V. nonalfalfae* cluster than *V. dahliae*. As hybrid genome structures may impede
299 truthful phylogenetic resolution (Linder & Rieseberg 2004), we hypothesized that a hybrid
300 origin of the *V. longisporum* mitochondrial genome caused the discrepancy between the
301 phylogenetic trees based on nuclear and mitochondrial DNA. In order to elucidate the hybrid
302 nature, differences in mitochondrial sequence identities of *V. longisporum* or *V. nonalfalfae*
303 compared with *V. dahliae* were used to determine the parental origin of *V. longisporum*
304 mitochondrial genomic regions (Figure 6). As *V. nonalfalfae* diverged more recently from *V.*
305 *dahliae* than species A1, yet before the divergence of *V. dahliae* and species D1, mtDNA that
306 originates from species A1 and D1 should have lower and higher sequence identity,
307 respectively, with *V. dahliae* than with *V. nonalfalfae*. Indeed, the *V. longisporum*
308 mitochondrial genome consists of sections with higher and lower identity to *V. dahliae* than to
309 *V. nonalfalfae* confirming the hybrid nature of the *V. longisporum* mitochondrial genome
310 (Figure 6). The hybrid nature of the *V. longisporum* mtDNA was furthermore confirmed with
311 a phylogenetic analysis based on a 3.5 kb region that displays 0.7% higher average sequence
312 identity to *V. dahliae* than to *V. nonalfalfae*. This mtDNA region placed *V. longisporum* in the

313 same phylogenetic position of species D1 with a divergence after the last common ancestor of
314 *V. dahliae*, *V. alfalfae* and *V. nonalfalfae* (Figure 6). In contrast, a *V. longisporum* mtDNA
315 region of the same length that has on average 0.4% lower sequence identity to *V. dahliae* than
316 *V. nonalfalfae* placed *V. longisporum* in the same phylogenetic position as species A1 (Figure
317 6). In conclusion, in addition to the nuclear genome, also the mtDNA of *V. longisporum*
318 displays a mosaic structure after recombination of the DNA of the two individual parents.

DISCUSSION

Divergent evolution often fixates genomic incompatibilities between populations, leading to reproductive isolation and eventually even speciation (Seehausen et al. 2014). *Verticillium* species A1 and D1 are distinct with a genome-wide nucleotide divergence of 7.6%, yet both species overcame putative incompatibilities and hybridized into a stable allodiploid (Depotter et al. 2016a). Conceivably, extensive genome alterations occurred after hybridization, facilitating the *V. longisporum* genome to reach a stable equilibrium. The dynamic nature of the *V. longisporum* genome during the hybridization aftermath is displayed by its mosaic structure, not only in the nuclear genome, but even in the mitochondrial genome (Figure 1). Mosaicism in *V. longisporum* is not driven by homogenization that played a negligible role in the hybridization aftermath (Figure 3). Rather, *V. longisporum* mosaic genome structure is caused by extensive genomic rearrangements after hybridization (Figure 4, S2). Genomic rearrangements are major drivers of evolution and facilitate adaptation to novel or changing environments (Seidl & Thomma 2014). This mode of evolution is not specific to the hybrid nature of *V. longisporum* as *V. dahliae* similarly encountered extensive chromosomal reshuffling (de Jonge et al. 2013; Faino et al. 2016). In *V. dahliae*, genomic rearrangements are associated with the occurrence of lineage-specific regions that are derived from segmental duplications, and that are crucial for fungal aggressiveness as they are enriched for transcribed transposable elements and *in planta*-expressed genes (de Jonge et al. 2013; Faino et al. 2016). Genomic rearrangements often result from double-strand DNA breaks that are erroneously repaired based on templates that display high sequence similarity (Seidl & Thomma 2014). As expected, the majority of the synteny breaks between the genomes of *V. longisporum* strains VLB2 and VL20 reside in repeat-rich genome regions (Figure S3) as, due to their abundance, repetitive sequences are more likely to act as a substrate for unfaithful repair (Seidl & Thomma 2014). Nevertheless, 43% of the synteny breaks identified in *V. longisporum* are not

associated with repeat-rich regions. However, the presence of two genomes provides orthologous sequences with sufficient identity to mediate unfaithful repair. Double-strand DNA breaks can be generated by transposable elements (TEs). Transposon activity is typically constrained by epigenetic mechanisms such as DNA methylations. However, these constrained may be alleviated upon genome challenges, such as allopolyploidization (Slotkin & Martienssen 2007). The "genome-shock" that *V. longisporum* encountered upon hybridization may have induced TE activity. The higher repeat content of the *V. longisporum* genome compared to the haploid *V. dahliae* may suggest that TE proliferation occurred after hybridization, leading to a modest genome expansion, resulting in a genome size of *V. longisporum* that is more than double when compared with *V. dahliae*, whereas *V. longisporum* contains only 90% more genes (Table 1). Similarly, it has been suggested that hybridization led to TE proliferation in allopolyploid root-knot nematodes, *Meloidogyne* spp., as TEs cover a ±1.7 times higher proportion of their genomes when compared with the closely related, yet non-hybrid, *Meloidogyne hapla* (Blanc-Mathieu et al. 2017).

Whole-genome duplication events are usually followed by extensive gene loss, often leading to reversion to the original ploidy state (Maere et al. 2005). However, the so-called 'haploidization' of *V. longisporum* has only proceeded to a limited extent, as 80% of the genes are present in two copies (Figure 2), whereas the haploid *V. dahliae* genome contains only 1% of its genes in two copies. Perhaps *V. longisporum* hybridized only recently, with gene-loss being an on-going process that by now has only progressed marginally, but that will lead to further losses over time. Alternatively, the retention of genes in two copies is of an evolutionary advantage, as the two copies make an additive contribution or their redundancy provides a source for functional divergence (Gu et al. 2002; Blanc & Wolfe 2014). Furthermore, the majority of the two parental genomes may also be retained to maintain

368 genomic balance, as stoichiometric difference of in interacting genes may have detrimental
369 outcomes (Birchler & Veitia 2012).

370 Hybridization can lead to incongruences between phylogenetic trees based on genome
371 sections of different parental origin (Linder & Rieseberg 2004). High-resolution tree
372 construction showed that species A1 diverged before the last common ancestor of *V. alfalfae*,
373 *V. dahliae* and *V. nonalfalfae*, whereas species D1 only recently diverged from *V. dahliae* as
374 previously reported (Inderbitzin et al. 2011a). Intriguingly, the phylogenetic positions of the
375 parental genomes did not correspond to that of the mitochondrial genome of *V. longisporum*
376 (Figure 6). Mitochondrial DNA is subjected to laws different from the Mendelian principles
377 of segregation and independent assortment as it is maternally inherited in most sexual
378 eukaryotes, including numerous fungal species (Basse 2010). However, for particular
379 organisms, bi-parental mitochondrial inheritance is common. For instance, in *S. cerevisiae*
380 heteroplasmy can be maintained for ~20 generations, allowing parental mitochondrial
381 genomes to recombine (Fritsch et al. 2014). The mitochondrial genome of *V. longisporum* has
382 been inherited bi-parentally, as the mitochondrial genome is a mosaic consisting of alternating
383 regions derived from the A1 or D1 parent (Figure 6). Similar to *V. longisporum*, two incipient
384 species of the budding yeast *Saccharomyces paradoxus* contributed to the mitochondrial
385 genome of their natural hybrid offspring (Leducq et al. 2017). Bi-parental inheritance is often
386 associated with hybridization, although it is uncertain if hybridization facilitates paternal
387 leakage or if bi-parental inheritance is a common phenomenon that is easer to detect in
388 hybrids (Barr et al. 2005).
389

390 **Conclusion**

391 The *V. longisporum* genome consists of two near to complete genomes of its haploid parents.
392 Rearrangements between these parental chromosome sets occurred, resulting in a mosaic

genome structure. *V. longisporum* genomes display high plasticity, as 60 synteny breaks were confirmed between strains with high nucleotide identity. Conceivably, the absence of meiotic constraints and the presence of orthologous DNA clusters provide ample opportunities for the *V. longisporum* genome to recombine. Inter-parental genomic recombination and functional diversification of homeologs give *V. longisporum* an additional potential to adapt to environmental alterations, which haploid *Verticillium* spp. do not have. This may have enabled *V. longisporum* to alter its host range and cause disease on Brassicaceous plants.

ACKNOWLEDGEMENTS

The authors would like to thank the Marie Curie Actions programme of the European Commission that financially supported the research of J.R.L.D. Work in the laboratories of B.P.H.J.T. and M.F.S is supported by the Research Council Earth and Life Sciences (ALW) of the Netherlands Organization of Scientific Research (NWO).

REFERENCES

Bao W, Kojima KK, Kohany O. 2015. Repbase Update, a database of repetitive elements in eukaryotic genomes. Mob. DNA. 6:11.

Barker MS, Arrigo N, Baniaga AE, Li Z, Levin DA. 2015. On the relative abundance of autopolyploids and allopolyploids. New Phytol. 210:391–398.

Barr CM, Neiman M, Taylor DR. 2005. Inheritance and recombination of mitochondrial genomes in plants, fungi and animals. New Phytol. 168:39–50.

Basse CW. 2010. Mitochondrial inheritance in fungi. Curr. Opin. Microbiol. 13:712–719.

te Beest M et al. 2012. The more the better? The role of polyploidy in facilitating plant invasions. Ann. Bot. 109:19–45.

Birchler JA, Veitia RA. 2012. Gene balance hypothesis: connecting issues of dosage sensitivity across biological disciplines. Proc. Natl. Acad. Sci. 109:14746–14753.

Blanc-Mathieu R et al. 2017. Hybridization and polyploidy enable genomic plasticity without sex in the most devastating plant-parasitic nematodes. PLoS Genet. 13:e1006777.

Blanc G, Wolfe KH. 2004. Functional divergence of duplicated genes formed by polyploidy during Arabidopsis evolution. Plant Cell. 16:1679–1691.

Brasier CM, Kirk SA. 2001. Comparative aggressiveness of standard and variant hybrid alder phytophthoras, *Phytophthora cambivora* and other *Phytophthora* species on bark of *Alnus*, *Quercus* and other woody hosts. Plant Pathol. 50:218–229.

Campbell MA, Ganley ARD, Gabaldón T, Cox MP. 2016. The case of the missing ancient fungal polyploids. Am. Nat. 188:602–614.

Cook DE, Mesarich CH, Thomma BPHJ. 2015. Understanding plant immunity as a surveillance system to detect invasion. Annu. Rev. Phytopathol. 53:541–563.

Depotter JRL, Deketelaere S, et al. 2016a. *Verticillium longisporum* , the invisible threat to oilseed rape and other brassicaceous plant hosts. Mol. Plant Pathol. 17:1004–1016.

431 Depotter JRL, Rodriguez-Moreno L, Thomma BPHJ, Wood TA. 2017a. The emerging British
432 *Verticillium longisporum* population consists of aggressive *Brassica* pathogens.
433 Phytopathology. 107:1399-1405.
434 Depotter JRL, Seidl MF, van den Berg GCM, Thomma BPHJ, Wood TA. 2017b. A distinct
435 and genetically diverse lineage of the hybrid fungal pathogen *Verticillium longisporum*
436 population causes stem striping in British oilseed rape. Environ. Microbiol. 19:3997–4009.
437 Depotter JRL, Seidl MF, Wood TA, Thomma BPHJ. 2016b. Interspecific hybridization
438 impacts host range and pathogenicity of filamentous microbes. Curr. Opin. Microbiol. 32:7–
439 13.
440 Doyle JJ et al. 2008. Evolutionary genetics of genome merger and doubling in plants. Annu.
441 Rev. Genet. 42:443–461.
442 Faino L et al. 2015. Single-molecule real-time sequencing combined with optical mapping
443 yields completely finished fungal genome. MBio. 6:e00936-15.
444 Faino L et al. 2016. Transposons passively and actively contribute to evolution of the two-
445 speed genome of a fungal pathogen. Genome Res. 26:1091–1100.
446 Fogelqvist J et al. 2018. Analysis of the hybrid genomes of two field isolates of the soil-borne
447 fungal species *Verticillium longisporum*. BMC Genomics. 19:14.
448 Fritsch ES, Chabbert CD, Klaus B, Steinmetz LM. 2014. A genome-wide map of
449 mitochondrial DNA recombination in yeast. Genetics. 198:755–771.
450 Gibson B, Liti G. 2015. *Saccharomyces pastorianus*: genomic insights inspiring innovation
451 for industry. Yeast. 32:17–27.
452 Gu Z, Nicolae D, Lu H-S, Li W-H. 2002. Rapid divergence in expression between duplicate
453 genes inferred from microarray data. Trends Genet. 18:609–613.
454 Hoff KJ, Lange S, Lomsadze A, Borodovsky M, Stanke M. 2016. BRAKER1: unsupervised
455 RNA-seq-based genome annotation with GeneMark-ET and AUGUSTUS. Bioinformatics.

32:767–769.

Husson C et al. 2015. Evidence for homoploid speciation in *Phytophthora alni* supports taxonomic reclassification in this species complex. Fungal Genet. Biol. 77:12–21.

Inderbitzin P, Bostock RM, et al. 2011a. Phylogenetics and taxonomy of the fungal vascular wilt pathogen *Verticillium*, with the descriptions of five new species. PLoS One. 6:e28341.

Inderbitzin P, Davis RM, Bostock RM, Subbarao KV. 2011b. The ascomycete *Verticillium longisporum* is a hybrid and a plant pathogen with an expanded host range. PLoS One. 6:e18260.

Jelen V, de Jonge R, Van de Peer Y, Javornik B, Jakše J. 2016. Complete mitochondrial genome of the Verticillium-wilt causing plant pathogen *Verticillium nonalfalfae*. PLoS One. 11:e0148525.

de Jonge R et al. 2013. Extensive chromosomal reshuffling drives evolution of virulence in an asexual pathogen. Genome Res. 23:1271–1282.

Katoh K, Misawa K, Kuma K, Miyata T. 2002. MAFFT: a novel method for rapid multiple sequence alignment based on fast Fourier transform. Nucleic Acids Res. 30:3059–3066.

Katoh K, Standley DM. 2013. MAFFT multiple sequence alignment software version 7: improvements in performance and usability. Mol. Biol. Evol. 30:772–780.

Kurtz S et al. 2004. Versatile and open software for comparing large genomes. Genome Biol. 5:R12.

Langmead B, Salzberg SL. 2012. Fast gapped-read alignment with Bowtie 2. Nat Methods. 9:357–359.

Leducq J-B et al. 2017. Mitochondrial recombination and introgression during speciation by hybridization. Mol. Biol. Evol. 34:1947–1959.

Li H et al. 2009. The Sequence Alignment/Map format and SAMtools. Bioinformatics. 25:2078–2079.

481 Linder CR, Rieseberg LH. 2004. Reconstructing patterns of reticulate evolution in plants.
482 Am. J. Bot. 91:1700–1708.
483 Lohaus R, Van de Peer Y. 2016. Of dups and dinos: evolution at the K/Pg boundary. Curr.
484 Opin. Plant Biol. 30:62–69.
485 Lomsadze A, Burns PD, Borodovsky M. 2014. Integration of mapped RNA-Seq reads into
486 automatic training of eukaryotic gene finding algorithm. Nucleic Acids Res. 42:e119.
487 Louis VL et al. 2012. *Pichia sorbitophila* , an interspecies yeast hybrid, reveals early steps of
488 genome resolution after polyploidization. G3. 2:299–311.
489 Maere S et al. 2005. Modeling gene and genome duplications in eukaryotes. Proc. Natl. Acad.
490 Sci. 102:5454–5459.
491 Mallet J. 2005. Hybridization as an invasion of the genome. Trends Ecol. Evol. 20:229–237.
492 Marcet-Houben M, Gabaldón T. 2015. Beyond the whole-genome duplication: phylogenetic
493 evidence for an ancient interspecies hybridization in the baker's yeast lineage. PLOS Biol.
494 13:e1002220.
495 Matute DR, Butler IA, Turissini DA, Coyne JA. 2010. A test of the snowball theory for the
496 rate of evolution of hybrid incompatibilities. Science. 329:1518–1521.
497 McGrath CL, Gout J-F, Johri P, Doak TG, Lynch M. 2014. Differential retention and
498 divergent resolution of duplicate genes following whole-genome duplication. Genome Res.
499 24:1665–1675.
500 Mixão V, Gabaldón T. 2018. Hybridization and emergence of virulence in opportunistic
501 human yeast pathogens. Yeast. 35:5-20.
502 Novakazi F et al. 2015. The three lineages of the diploid hybrid *Verticillium longisporum*
503 differ in virulence and pathogenicity. Phytopathology. 105:662–673.
504 Ortiz-Merino RA et al. 2017. Evolutionary restoration of fertility in an interspecies hybrid
505 yeast, by whole-genome duplication after a failed mating-type switch. PLOS Biol.

15:e2002128.

Van de Peer Y, Mizrachi E, Marchal K. 2017. The evolutionary significance of polyploidy. Nat. Rev. Genet. 18:411-424.

Peris D et al. 2017. Hybridization and adaptive evolution of diverse *Saccharomyces* species for cellulosic biofuel production. Biotechnol. Biofuels. 10:78.

Phanstiel DH, Boyle AP, Araya CL, Snyder MP. 2014. Sushi.R: flexible, quantitative and integrative genomic visualizations for publication-quality multi-panel figures. Bioinformatics. 30:2808–2810.

Quinlan AR, Hall IM. 2010. BEDTools: a flexible suite of utilities for comparing genomic features. Bioinformatics. 26:841–842.

Robinson JT et al. 2011. Integrative Genomics Viewer. Nat. Biotechnol. 29:24–26.

Seehausen O et al. 2014. Genomics and the origin of species. Nat. Rev. Genet. 15:176–192.

Seidl MF, Thomma BPHJ. 2014. Sex or no sex: Evolutionary adaptation occurs regardless. BioEssays. 36:335–345.

Shi-Kunne X, Faino L, van den Berg GCM, Thomma BPHJ, Seidl MF. Evolution within the fungal genus *Verticillium* is characterized by chromosomal rearrangements and gene losses. Environ. Microbiol. Accepted

Short DPG, Gurung S, Hu X, Inderbitzin P, Subbarao KV. 2014. Maintenance of sex-related genes and the co-occurrence of both mating types in *Verticillium dahliae*. PLoS One. 9:e112145.

Simão FA, Waterhouse RM, Ioannidis P, Kriventseva EV, Zdobnov EM. 2015. BUSCO: assessing genome assembly and annotation completeness with single-copy orthologs. Bioinformatics. 31:3210–3212.

Simms D, Cizdziel P, Chomczynski P. 1993. TRIzol: a new reagent for optimal single-step isolation of RNA. Focus. 15:99–102.

Slotkin RK, Martienssen R. 2007. Transposable elements and the epigenetic regulation of the genome. Nat. Rev. Genet. 8:272–285.

Smit AFA, Hubley R, Green P. 2015. RepeatMasker Open-4.0. Available from: http://www.repeatmasker.org

Stamatakis A. 2014. RAxML version 8: A tool for phylogenetic analysis and post-analysis of large phylogenies. Bioinformatics. 30:1312–1313.

Stanke M, Diekhans M, Baertsch R, Haussler D. 2008. Using native and syntenically mapped cDNA alignments to improve de novo gene finding. Bioinformatics. 24:637–644.

Stukenbrock EH, Christiansen FB, Hansen TT, Dutheil JY, Schierup MH. 2012. Fusion of two divergent fungal individuals led to the recent emergence of a unique widespread pathogen species. Proc. Natl. Acad. Sci. 109:10954–9.

Trapnell C, Pachter L, Salzberg SL. 2009. TopHat: discovering splice junctions with RNA-Seq. Bioinformatics. 25:1105–1111.

Vanneste K, Baele G, Maere S, Van de Peer Y. 2014a. Analysis of 41 plant genomes supports a wave of successful genome duplications in association with the Cretaceous-Paleogene boundary. Genome Res. 24:1334–1347.

Vanneste K, Maere S, Van de Peer Y. 2014b. Tangled up in two: a burst of genome duplications at the end of the Cretaceous and the consequences for plant evolution. Philos. Trans. R. Soc. B Biol. Sci. 369:20130353.

Zeise K, Tiedemann Av. 2002. Host specialization among vegetative compatibility groups of *Verticillium dahliae* in relation to *Verticillium longisporum*. J. Phytopathol. 150:112–119.

TABLES

Table 1: Comparison *V. longisporum* and *V. dahliae* genomes.

	V. longisporum **VLB2**	***V. longisporum*** **VL20**	***V. dahliae*** **JR2**
Genome size	72.9 Mb	72.3 Mb	36.2 Mb
Number of contigs	45	44	8
Complete chromosomes	6	4	8
Number of genes	19,123	18,784	9,909
Telomere regions	29	30	16
Repeat content	14.28	13.90	6.49
BUSCO completeness	99.0%	98.3%	98.7%

554 **FIGURE LEGENDS**

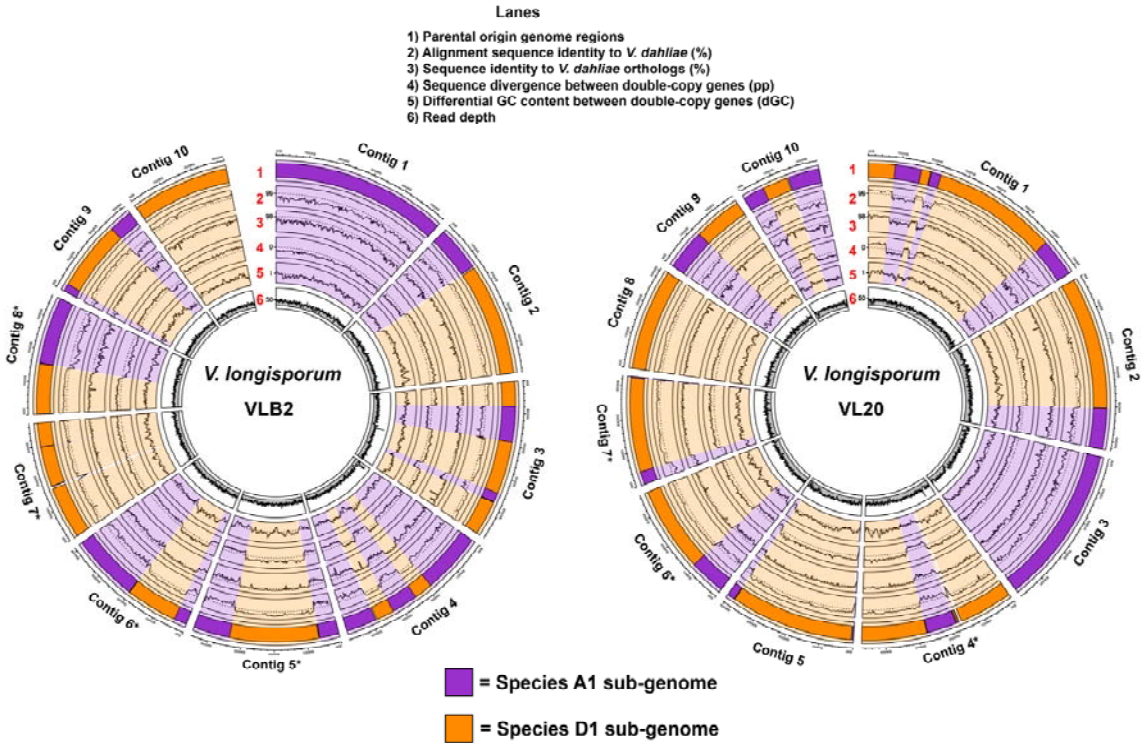

555

556 **Fig. 1: Determination of parental origin of *Verticillium longisporum* genome sections**.
557 The ten largest contigs of the genome assemblies of *V. longisporum* strains VLB2 and VL20
558 are depicted. Lane 1: regions with a sequence identity of at least 96% were assigned to
559 Species D1 (orange), whereas ones with lower sequence identity to Species A1 (purple). Lane
560 2: sequence identity of *V. longisporum* alignments to *V. dahliae*. Lane 3: Sequence identity
561 between exonic regions of *V. longisporum* and *V. dahliae* orthologs. Lane 4: Difference in
562 sequence identity in percent point (pp) between exonic regions of *V. longisporum* double-
563 copy genes. Only gene pairs with an ortholog in *V. dahliae* are depicted. Alleles with a higher
564 identity to *V. dahliae* are depicted as a positive pp difference, whereas the corresponding
565 homolog as a negative pp difference. Lane 5: the relative difference in GC content (dGC)
566 between genes in double copy. Lane 6: Read depth with non-overlapping windows of 10 kb.
567 Data points of lanes 3-5 represent the average value of a window of eleven genes, which
568 proceed with a step of one gene.

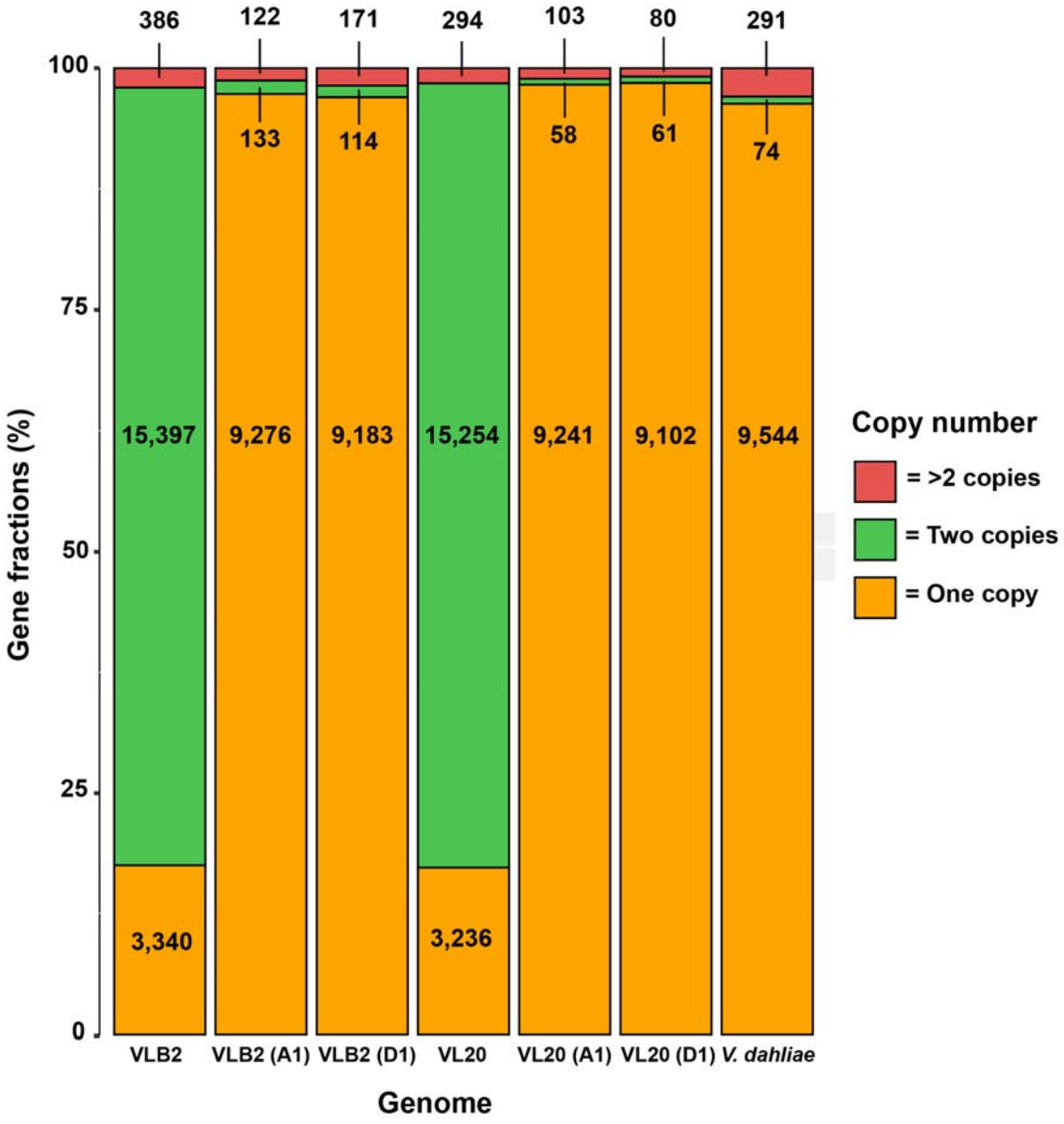

Fig. 2: Gene copy number distribution within *Verticillium* (sub-)genomes. "(A1)" and "(D1)" represent species A1 and D1 sub-genomes, respectively, of the *V. longisporum* strains VLB2 and VL20. For *V. dahliae*, the strain JR2 was used.

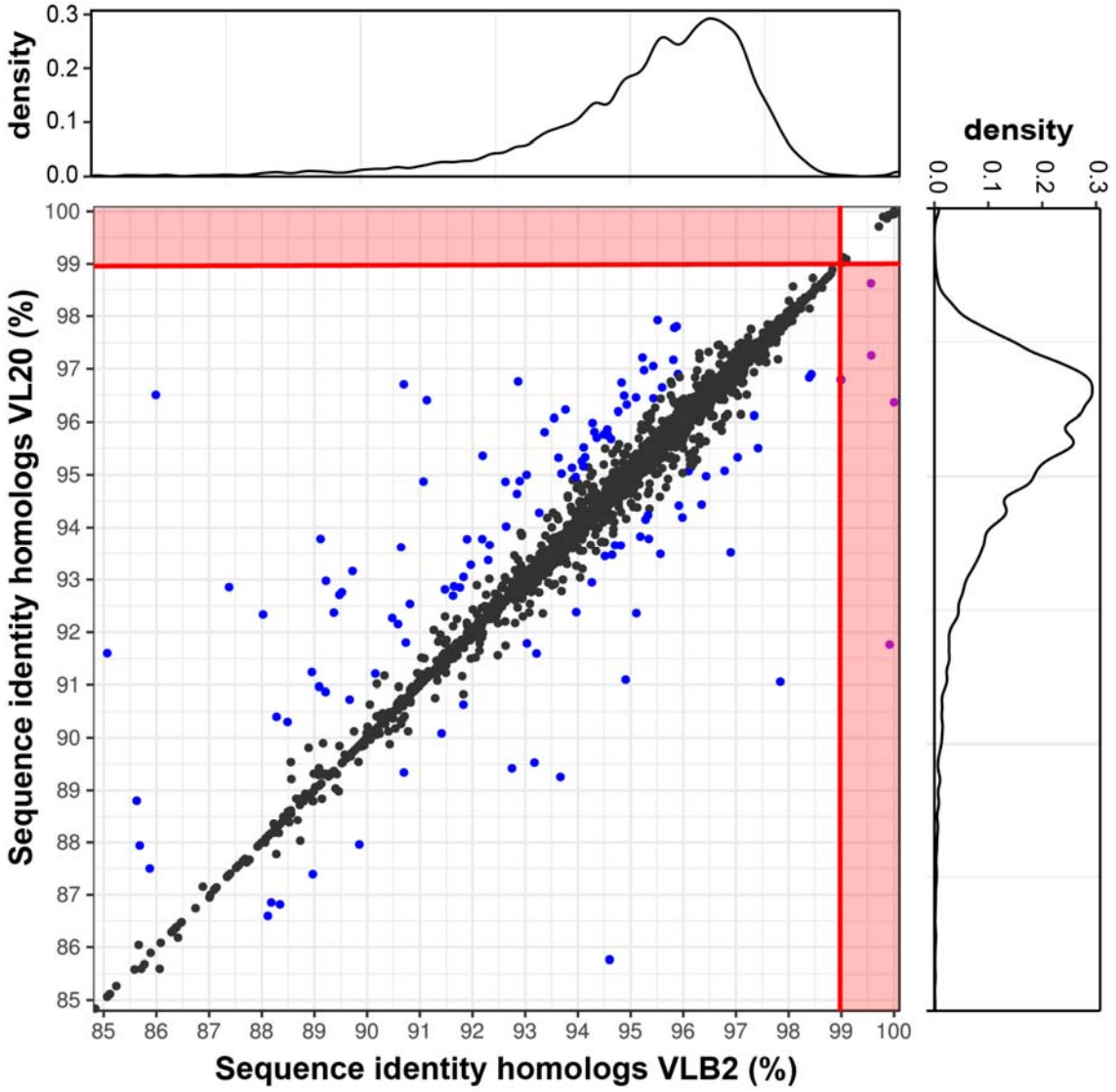

Fig. 3: The contribution of gene conversion to *V. longisporum* genome evolution. Sequence identities between double-copy genes, present in *V. longisporum* VLB2 and VL20, are depicted. Gene pairs that encountered gene conversion (purple dots in the red zones) have sequence divergence of more than one percent in one *V. longisporum* strain and less than one percent in the other strain. In other cases, pairs that differ less than one percent are depicted as a black dot, whereas a difference higher than one percent is depicted as a blue dot.

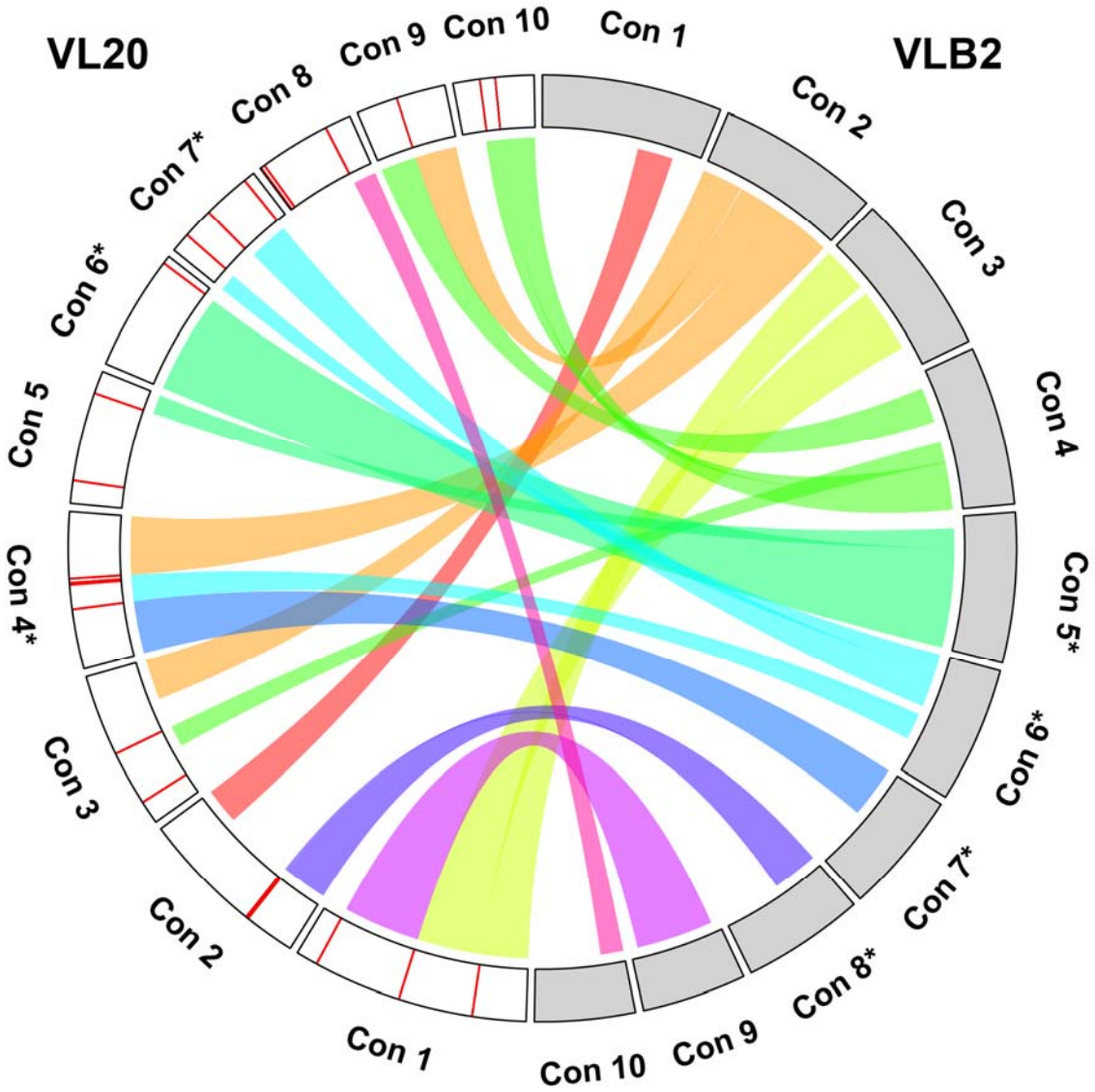

582

583 **Fig. 4: The contribution of genomic rearrangements to *V. longisporum* genome**
584 **evolution.** The ten largest contigs of the *V. longisporum* strains VLB2 (displayed in grey) and
585 VL20 (displayed in white) are depicted with complete chromosomes indicated by asterisks.
586 Ribbons indicate syntenic genome regions between the two strains. Red bars on the contigs
587 indicate synteny breaks that are confirmed by discontinuity in alignment of VLB2 reads to
588 VL20 genome.

589

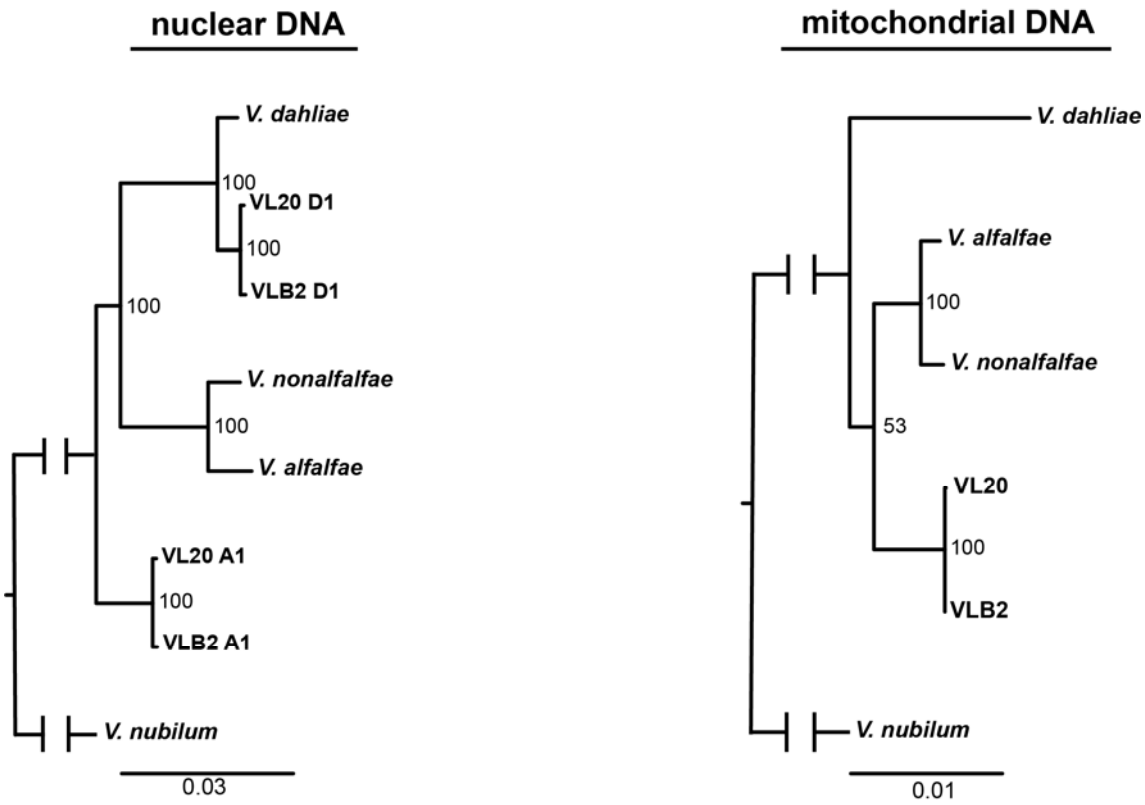

590

591 **Fig. 5: Phylogenetic positioning of *Verticillium longisporum* nuclear sub-genomes and**
592 **mitochondrial genome to other *Verticillium* species of clade Flavnonexudans.** The nuclear
593 phylogenetic tree was constructed with 1,194 orthologous genes, whereas the mitochondrial
594 phylogenetic tree was based on complete mitochondrial genomes. Maximum-likelihood
595 phylogeny analysis of *Verticillium* spp. was rooted on *Verticillium nubilum* and the robustness
596 of the tree was assessed using 100 bootstrap replicates.

597

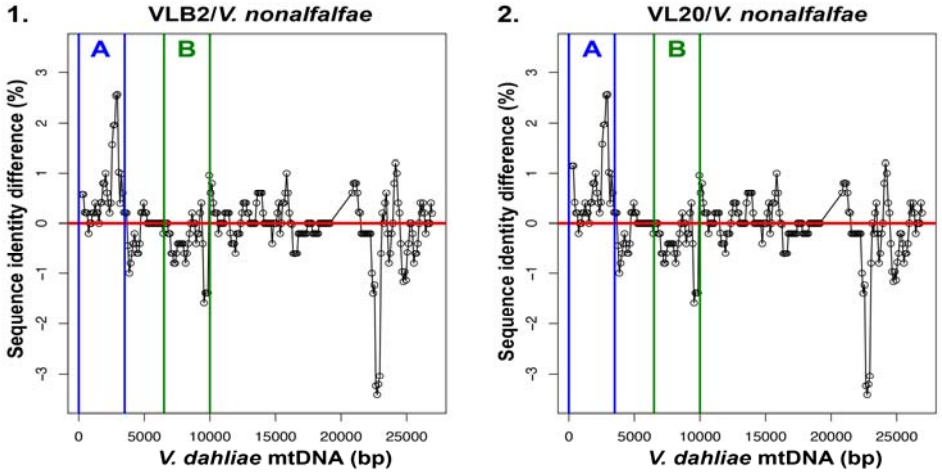

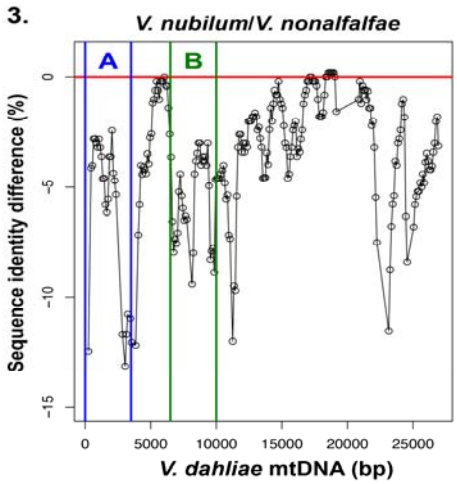

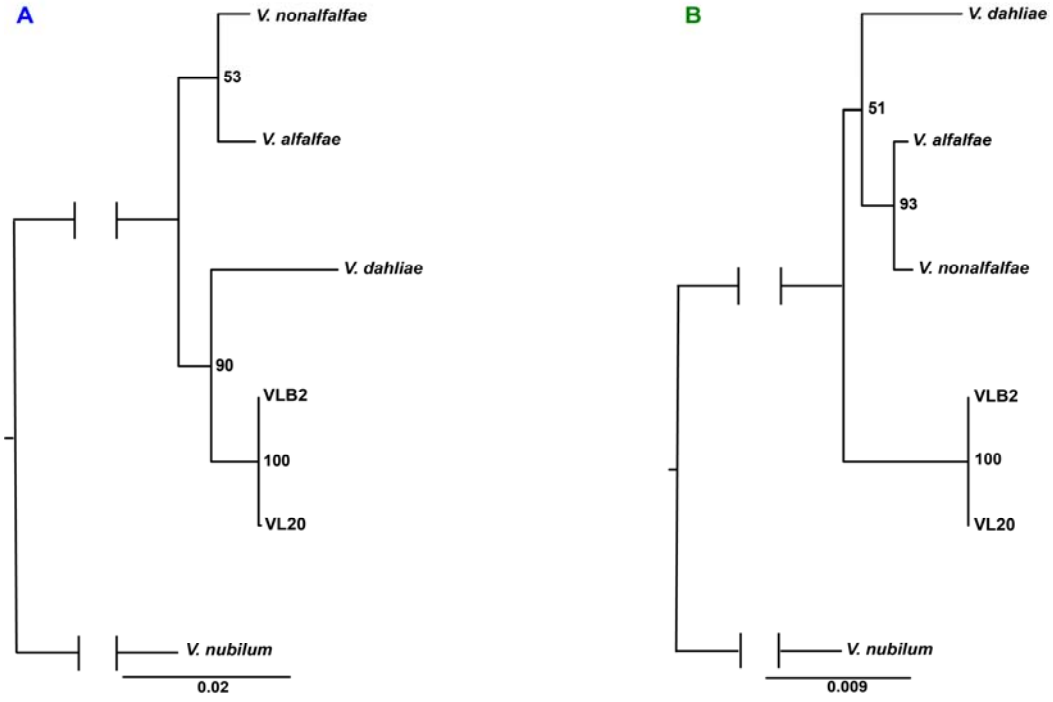

598

599 **Fig. 6: The bi-parental origin to mitochondrial genome of *Verticillium longisporum*.** The
600 *V. dahliae* mitochondrial genome was divided in 500 bp sliding windows with 100 bp steps.
601 The differences in sequence identity of these windows with other *Verticillium* genomes were
602 determined for: 1. *V. longisporum* strain VLB2 and *V. nonalfalfae*, 2. *V. longisporum* strain
603 VL20 and *V. nonalfalfae*, and 3. *V. nubilum* and *V. nonalfalfae*. The two phylogenetic trees
604 are constructed with maximum-likelihood based on region A and B of the mitochondrial *V.*
605 *dahliae* genome, both 3.5 kb in size. The phylogenetic trees were rooted on *Verticillium*
606 *nubilum* and the robustness of the tree was assessed using 100 bootstrap replicates.

607 **SUPPLEMENTARY MATERIAL**

608 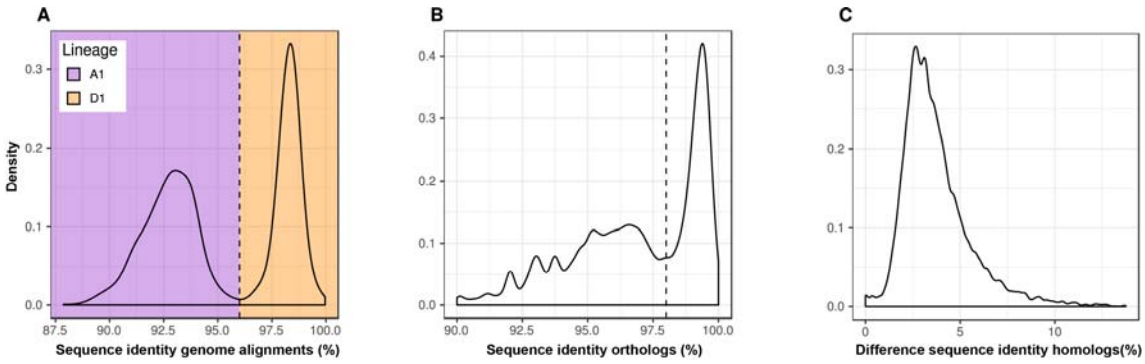

609 **Fig. S1: Lines of evidence for the parental origin of *V. longisporum* genomic regions.** (A)
610 Distribution of sequence identity of *V. longisporum* alignments to *V. dahliae*. (B) The
611 distribution of the sequence identity between *V. longisporum* exonic regions of genes and
612 their *V. dahliae* orthologs. (C) Distribution of sequence identity between exonic regions of *V.*
613 *longisporum* homologs that are present in two copies. Strains VLB2 and JR2 were used for *V.*
614 *longisporum* and *V. dahliae*, respectively.

615

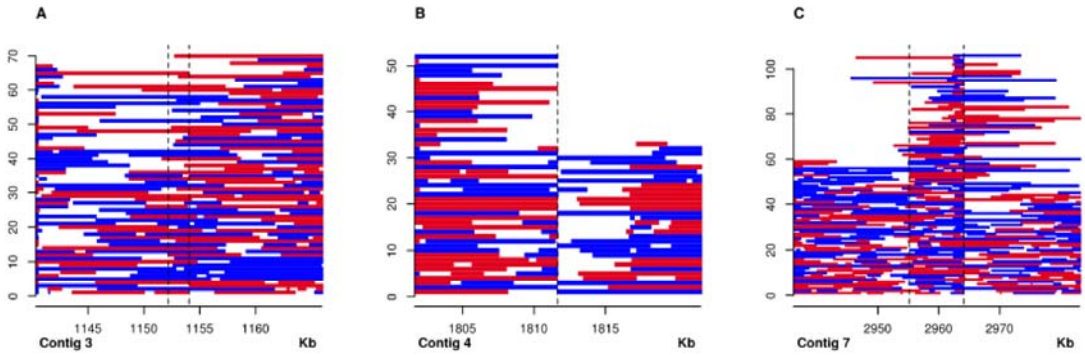

Fig. S2: Synteny break confirmation by mapping *V. longisporum* VLB2 reads to the VL20 genome. Red and blue bars represent forward and reverse aligned VLB2 reads to the VL20 genome. The dashed lines show the suggested position in synteny break through genome alignment. (A) In particular cases, read alignments did not confirm the break in synteny. (B) In other cases, breaks in synteny were confirmed as reads abruptly stopped and started on these genome positions. (C) Breaks were also considered truthful if regions showed overlap in repeat-rich regions where read overlap between adjacent genome regions is lacking.

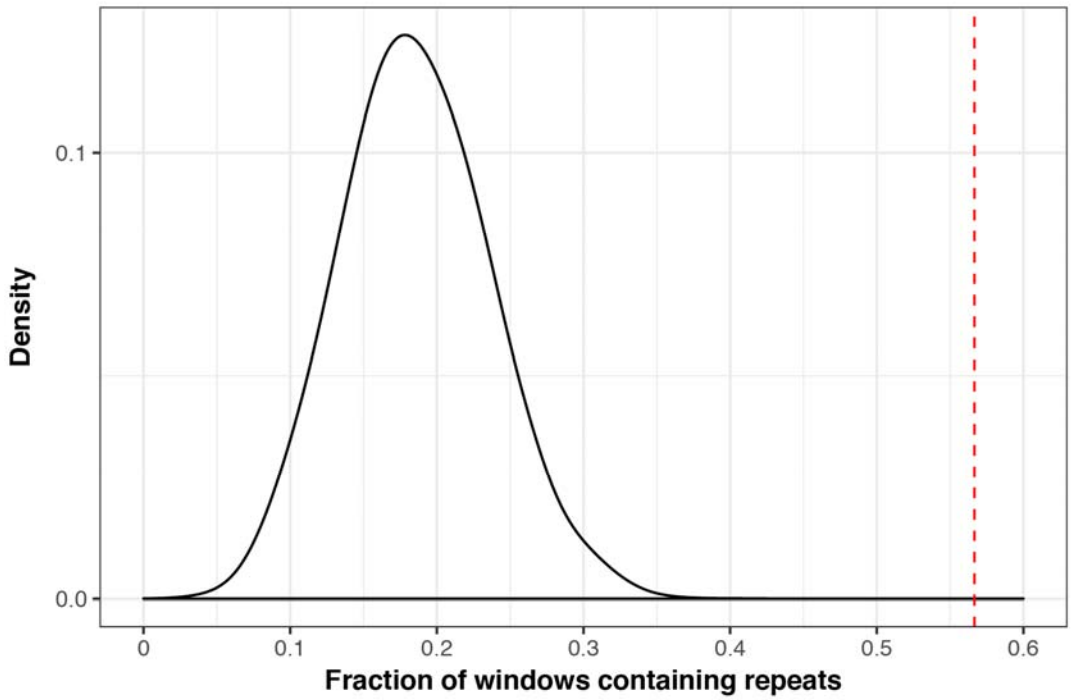

626

627 **Fig. S3: The association of synteny breaks with repetitive elements.** The black curve
628 represents the fraction of 60 randomly chosen 1 kb windows in the *V. longisporum* VL20 that
629 are repeat-rich, which has been permutated 10,000 times. The red line indicates the fraction of
630 true breaks that lay in a 1 kb window enriched for repeats (57%).